THE JOURNAL OF BIOLOGICAL CHEMISTRY VOL. 288, NO. 14, pp. 9742–9754, April 5, 2013


# Dynamics of the Rhomboid-like Protein RHBDD2 Expression in Mouse Retina and Involvement of Its Human Ortholog in Retinitis Pigmentosa*

Received for publication, September 21, 2012, and in revised form, January 29, 2013 Published, JBC Papers in Press, February 5, 2013, DOI 10.1074/jbc.M112.419960

**Novruz B. Ahmedli[‡1], Yekaterina Gribanova[‡], Collins C. Njoku[‡], Akash Naidu[‡], Alejandra Young[‡], Emmanuel Mendoza[‡], Clyde K. Yamashita[‡], Riza Köksal Özgül[§], Jerry E. Johnson[¶], Donald A. Fox[‖**‡‡], and Debora B. Farber[‡§§¶¶]**

*From the [‡]Jules Stein Eye Institute, [§§]Molecular Biology Institute, and [¶¶]Brain Research Institute, UCLA, Los Angeles, California 90095, [§]Department of Molecular Biology, Hacettepe University, 06230 Beytepe-Ankara, Turkey, [¶]Department of Natural Sciences, University of Houston-Downtown, Houston, Texas 77002, and [‖]College of Optometry, **Department of Biology and Biochemistry, and [‡‡]Department of Pharmacology and Pharmaceutical Sciences, University of Houston, Houston, Texas 77004*

**Background:** RHBDD2 is distantly related to rhomboids, membrane-bound proteases.
**Results:** In retina, RHBDD2 exists as a monomer in all cells throughout life and a homotrimer only in cone outer segments; a mutation in RHBDD2 possibly leads to retinitis pigmentosa.
**Conclusion:** RHBDD2 plays important roles in development and normal retinal function.
**Significance:** This is the first characterization of RHBDD2 and its association with retinal disease.

**The novel rhomboid-like protein RHBDD2 is distantly related to rhomboid proteins, a group of highly specialized membrane-bound proteases that catalyze regulated intramembrane proteolysis. In retina, RHBDD2 is expressed from embryonic stages to adulthood, and its levels show age-dependent changes. RHBDD2 is distinctly abundant in the perinuclear region of cells, and it localizes to their Golgi. A glycine zipper motif present in one of the transmembrane domains of RHBDD2 is important for its packing into the Golgi membranes. Its deletion causes dislodgment of RHBDD2 from the Golgi. A specific antibody against RHBDD2 recognizes two forms of the protein, one with low (39 kDa; $RHBDD2_L$) and the other with high (117 kDa; $RHBDD2_H$) molecular masses in mouse retinal extracts. $RHBDD2_L$ seems to be ubiquitously expressed in all retinal cells. In contrast, $RHBDD2_H$ seems to be present only in the outer segments of cone photoreceptors and may correspond to a homotrimer of $RHBDD2_L$. This protein consistently co-localizes with S- and M-types of cone opsins. We identified a homozygous mutation in the human *RHBDD2* gene, R85H, that co-segregates with disease in affected members of a family with autosomal recessive retinitis pigmentosa. Our findings suggest that the RHBDD2 protein plays important roles in the development and normal function of the retina.**

Highly specialized membrane-bound proteases, which cleave other membrane proteins within their membrane-spanning segments, have been intensively studied during the last decade. These enzymes are identifiable in nearly all the sequenced genomes of archaea, bacteria, eukaryotic organisms, and mitochondria. They influence diverse processes, including transcriptional control, cellular differentiation, lipid metabolism, mitochondrial membrane remodeling, parasite invasion, and bacterial protein translocation (1–6). Rhomboid proteins, widely conserved polytopic membrane proteins with six or seven transmembrane domains, are members of the intramembrane proteolytic protein family. The *rhomboid* gene was first discovered in *Drosophila* and is an important component of the epidermal growth factor (EGF) receptor signaling pathway during development (7–10). Rhomboids directly recognize their substrates *in vitro* (11), and their conserved Ser and His residues are essential for proteolytic activity (12). Their active site is situated close to the extracellular face of the membrane, which allows them to release effector domains to the cell exterior. Mainly, rhomboids cleave transmembrane segments of type I orientation (N termini outside the cell) (6) and regulate the location and topology of membrane proteins with great precision.

A simplified phylogenetic tree of the rhomboid family shows three major taxonomic groups: the rhomboids, inactive rhomboids (iRhoms),[2] and inactive rhomboid homologues (13). The eukaryotic active rhomboids are a major group consisting of presenilin-associated rhomboid-like (PARL)-type rhomboids, which are mitochondrial, and secretases (types A and B), which reside in the secretory pathway.

Rhomboid-like proteins that lack essential catalytic residues are identified as iRhoms. Their characteristic features are a

* This work was supported, in whole or in part, by National Institutes of Health Grants RO1 EY08285 (to D. B. F.), RO1 ES012482 (to D. A. F.), P30 EY000331 (to the Jules Stein Eye Institute), and T32 EY07024 and P30 EY07551 (to the University of Houston College of Optometry). This work was also supported by Hope for Vision and Oppenheimer Foundation grants (to N. B. A.).

[1] To whom correspondence should be addressed: Jules Stein Eye Inst., UCLA, 100 Stein Plaza, Los Angeles, CA 90095-7000. Tel.: 310-206-6935; E-mail: akhmedov@jsei.ucla.edu.

[2] The abbreviations used are: iRhom, inactive rhomboid; E, embryonic day; P, postnatal day; EGFP, enhanced green fluorescent protein; arRP, autosomal recessive retinitis pigmentosa; OCT, optimal cutting temperature medium; DIG, digoxigenin; BFA, brefeldin A; GCL, ganglion cell layer; ONL, outer nuclear layer; OS, outer segments.

large loop between transmembrane domains 1 and 2 and an extended cytoplasmic N terminus (13, 14). Little is known about their function. Other rhomboid-like homologues that lack catalytic residues but do not cluster with the iRhoms are scattered across evolution.

Rhomboids have been implicated in a variety of human diseases as a result of their distinct functions. As a component of the mechanism of parasitic invasion in toxoplasmosis and malaria, these cell surface molecules obligate human pathogens to invade the host cells by forming irreversible junctures between the plasma membrane of the invading parasite and the host cell (15–17). As another example, the mitochondrial Rhomboid-7 is required to cleave the precursor forms of both Pink1 and Omi, proteins that are mutated in Parkinson disease (18). In addition, an identified mutation in PARL may be associated with insulin resistance and type 2 diabetes (19). Recently, two independent groups reported that iRhom2 is required for tumor necrosis factor release in mice. iRhom2 interacts with TNF$\alpha$-converting enzyme and regulates shedding of soluble, active TNF$\alpha$. Thus, iRhom2 may represent an attractive therapeutic target for treating TNF$\alpha$-mediated diseases (20, 21).

The focus of this study is the novel intramembrane, growth/development-associated, rhomboid-like protein RHBDD2. Here we describe the distribution of *Rhbdd2* transcripts in mouse tissues and their developmental expression as well as that of the RHBDD2 protein in retina. We show that two forms of RHBDD2 are present in mouse retina and demonstrate that one of these forms is specifically expressed in cone photoreceptor outer segments. Most importantly, we report a novel recessive missense mutation in the *RHBDD2* gene, which maps to the human 7q11 locus, in members of a family affected with autosomal recessive retinitis pigmentosa (arRP). This mutation co-segregates with the disease and links the *RHBDD2* gene to the arRP phenotype.

## EXPERIMENTAL PROCEDURES

*Animals*—C57BL/6J mice were obtained from our colonies bred from stock originated at The Jackson Laboratory (Bar Harbor, ME). Mouse eyes were quickly enucleated after death, and the retinas were dissected and frozen. In addition, other tissues were obtained from these animals and immediately frozen. All experiments were conducted in accordance with the approved UCLA Animal Care and Use Committee protocol and the Association for Research in Vision and Ophthalmology statement for the use of animals in ophthalmic and vision research.

*Embryo Collection*—Pregnant C57BL/6 mice were sacrificed at 12.5, 15.5, and 18.5 days postcoitum, and embryos were removed from the embryonic sac. Theiler staging was used to confirm the phenotype of the 12.5-, 15.5-, and 18.5-day-postcoitum embryos. Embryonic heads were fixed and embedded in OCT for cryosectioning and immunohistochemistry, whereas embryonic eyes were collected for RNA extraction and quantitative PCR analysis. For the former experiments, embryo heads were fixed in 4% paraformaldehyde in 10 mM phosphate-buffered saline (PBS) overnight. The next day, the tissue was rinsed three times with PBS and infiltrated with 30% sucrose in PBS overnight at 4 °C with gentle rotation. The following day, embryonic heads were placed overnight in a 1:1 ratio of 30% sucrose in PBS to OCT. Heads were then embedded in OCT and stored at −80 °C. The embedded tissue was sectioned (10 $\mu$m) and used for immunohistochemistry experiments.

*RNA Isolation and Northern Blot Analysis*—Total RNA was extracted from mouse retinas (TRIzol, Invitrogen). Poly($A^+$) RNA was obtained with an mRNA purification kit (Oligotex, Qiagen, Valencia, CA). RNA was quantified with a NanoDrop ND-1000 spectrophotometer (NanoDrop Technologies, Wilmington, DE) and stored at −80 °C. Two micrograms of poly($A^+$) RNA were electrophoresed on 1.2% denaturing formaldehyde-agarose gels and transferred to a Hybond $N^+$ membrane (Amersham Biosciences). An 821-bp mouse retinal cDNA fragment containing part of the coding region and 3′-UTR was amplified with forward (5′-CTCATCTGACTCCAAGTTATC) and reverse (5′-AGAAGCCCAGGAGCCTCAAGAC) primers from the sequence of *Rhbdd2*, labeled with [$^{32}$P]dCTP, and used as a probe to hybridize the retinal and multiple mouse tissue (Ambion, Austin, TX) Northern blots.

*In Situ Hybridization*—*In situ* hybridization using 8-$\mu$m frozen sections of mouse retina embedded in OCT was performed as described previously (22). The same fragment of the mouse *Rhbdd2* cDNA used for Northern blot analysis was subcloned into the pCRII plasmid vector (Invitrogen) for generation of riboprobes. The antisense and sense digoxigenin (DIG)-labeled RNA riboprobes were synthesized with SP6 and T7 RNA polymerases (according to the DIG Labeling kit protocol, Roche Applied Science) and purified by spin columns (NucWay, Ambion). Sections were permeabilized with proteinase K (1 $\mu$g/ml). Prehybridization was performed at 70 °C for 30 min in a mixture of 50% formamide, 5× SSC (SSC: 150 mM NaCl, 15 mM sodium citrate, pH 4.5), 50 $\mu$g/ml yeast RNA, 50 $\mu$g/ml heparin, and 1% SDS. Hybridization occurred overnight at 70 °C in a humidified chamber. Sections were then washed with 5× SSC and 1% SDS in 50% formamide at 70 °C; 2× SSC in 50% formamide at 65 °C; and Tris-buffered saline, 0.1% Tween 20 at room temperature. Sections were incubated overnight at 4 °C with alkaline phosphatase-conjugated sheep anti-DIG antibody (1:200; Roche Applied Science) in 25 mM Tris-HCl, pH 7.5, 140 mM NaCl, 2.7 mM KCl, 1% Tween 20, 1% sheep serum; washed with TBST (140 mM NaCl, 2.7 mM KCl, 25 mM Tris-HCl, pH 7.5, 0.1% Tween 20); and incubated with nitroblue tetrazolium and 5-bromo-4-chloro-3-indolyl phosphate to visualize the mRNA. The reaction was stopped with acidic PBS containing 0.1% Tween 20.

*Quantitative Real Time RT-PCR and Statistical Analyses*—To analyze the levels of *Rhbdd2* transcripts, quantitative PCR was performed on first strand cDNAs. Primers were designed using Primer 3 Internet software (Whitehead Institute, Massachusetts Institute of Technology, Cambridge, MA) and synthesized by Integrated DNA Technology (San Diego, CA). The primer pair for total *Rhbdd2* mRNA was: forward, 5′-TCCCTCAGACCTCCTTCCTC and reverse, 5′-GTCAGATGAGGGTGGCAACTC. The primer pair for the long 3′-UTR *Rhbdd2* mRNA was: forward, 5′-GATGTGGGCTCTTAGGCAAG and reverse, 5-′ATCTAGGGGCAGTCCATCAG. Total RNA was isolated from embryonic eyes and retinal samples using the RNAqueous 4PCR protocol (Ambion) and treating twice with DNase I. RNA concentrations were measured using the

NanoDrop ND-1000 spectrophotometer, and 1 $\mu$g of RNA from each age was reverse transcribed. The quantitative PCRs were performed in SYBR Green Master Mix with the corresponding primer sets using a quantitative PCR system (MX3000P, Stratagene, La Jolla, CA). The melting curves of the PCR products were monitored to ensure that a single melting curve was obtained for each of the samples. To analyze the real time PCR data, signals from each sample were normalized to values obtained for $\beta$-actin cDNA, which was assayed simultaneously with the experimental samples. Analysis of variance using Monte Carlo bootstrapping was performed to analyze the possibility of a significant time effect in the expression of the total and long 3′-UTR *Rhbdd2* RNAs. Post hoc analyses were applied to determine significant changes in the total mRNA levels among the different age points. Bootstrap analysis was used because of the lack of a normal distribution in our data.

*Generation of Anti-RHBDD2 Antibody*—The RHBDD2 C-terminal peptide containing amino acids 344–360 (LGTPGATGSKESSKVAM) was synthesized and used to immunize rabbits for generation of the anti-RHBDD2 antibody. The obtained antibody (designated 7Rc) was affinity-purified (ProSci Inc., Poway, CA).

*Expression Construct*—To produce the full-length protein, the full-size *Rhbdd2* cDNA was amplified via RT-PCR from mouse retinal RNA using a primer set (5′-GGATCCATGGCGGCCCCGGGCCCCGCGAGT) and (5′-GAATTCCTTAGGGCAT GGCTACCTTGGAAGA) containing the desired restriction enzyme recognition sites (BamHI and EcoRI). The digested and purified PCR product (PCR gel extraction kit, Qiagen) was cloned into the pcDNA4/HisMax C vector between its BamHI/EcoRI cloning sites and sequenced for confirmation. The CMV promoter of this vector drove expression of the RHBDD2 fusion protein with the Xpress epitope at its N terminus.

*Site-directed Mutagenesis to Modify the Glycine Zipper Motif*—All glycine zipper motif mutant cDNAs were created using site-directed mutagenesis (QuikChange® II site-directed mutagenesis kit, Stratagene) to change the glycines in the zipper to leucines. S185L, G189L, G193L, and G197L are the single leucine substitution mutants (SSMs). In the triple substitution mutant, the Gly-189, Gly-193, and Gly-197 were collectively replaced with leucines. To delete 27 nucleotides from the glycine zipper motif sequence, two overlapping primers were made, each having 36 nucleotides. The forward primer consisted of 9 nucleotides upstream of the motif and 27 nucleotides downstream of the motif. The reverse primer had 27 nucleotides upstream of the motif and 9 nucleotides downstream. The two primers had an overlapping region of 18 nucleotides lacking the 9 amino acid residues of the motif. The PCR mixture was set up according to the QuikChange II XL site-directed mutagenesis kit. Once the PCR was completed, 10 units of DpnI were added, and the reaction mixture was incubated at 37 °C for 1 h to degrade the original plasmid used for PCR. EcoRI and BamHI sites were introduced into the 5′- and 3′-ends of the wild-type and mutant cDNAs to directionally subclone them into the pEGFP-N3 vector (BD Biosciences Clontech). The RHBDD2-EGFP fusion constructs were verified by sequencing. The list of specific primers used in site-directed mutagenesis is presented in Table 1.

*Transient and Stable Transfections*—HEK293 cells obtained from the American Type Culture Collection (Manassas, VA) were grown and transfected using the pcDNA4/HisMax-RHBDD2, each of the pEGFP-N3-RHBDD2 expression constructs, and the PolyFect transfection reagent (Qiagen). All experiments included the pcDNA4/HisMax plasmid without the insert as an internal normalization control. Transiently transfected cells were harvested for analysis of newly synthesized protein. Linearized plasmid was used to achieve stable transfection of HEK293 cells, and positive clones were selected (Zeocin, Invitrogen).

*Protein Extraction and Immunoblot Analysis*—Nuclear and cytoplasmic protein extracts from transfected cells, mouse retinas, and mouse brains were prepared using nuclear and cytoplasmic extraction reagents (NE-PER, Pierce). For total protein extraction, the harvested cells and tissue samples were lysed with lysis buffer (50 mM Tris-HCl, pH 7.5, 150 mM NaCl, 10% (w/v) glycerol, 100 mM NaF, 10 mM EGTA, 1 mM $Na_3VO_4$, 1% (w/v) Triton X-100, 5 $\mu$M $ZnCl_2$) and the Complete EDTA-free protease inhibitor mixture (Roche Applied Science) and then centrifuged at 10,000 × *g* for 20 min at 4 °C. Fifty micrograms of the extracted proteins were separated by SDS-PAGE on 7.5% gels (Pierce). Blots were incubated with primary antibody (1:7000 dilution) and secondary anti-rabbit IgG antibodies labeled with alkaline phosphatase (1:5000 dilution; Vector Laboratories). Western blots were visualized with either of two kits (the Amplified-Alkaline Phosphatase kit from Bio-Rad or the enhanced chemiluminescence (ECL) kit from Amersham Biosciences).

**TABLE 1**

**The sequences of the PCR primers used to obtain the 7R mutants**

Mutated codons are in bold. TSM, triple substitution mutant; GZMD, glycine zipper motif (amino acids 189–197) deletion mutant.

| Mutants | Primer name | Primer sequence (5′–3′) |
|---|---|---|
| SSM/S185L | m7R 4F | CAGACCTCCTTCCTC**CTT**AACGTCTCTGGCCTT |
| | m7R 4R | AAGGCCAGAGACGTT**AAG**GAGGAAGGAGGTCTG |
| SSM/G189L | m7R 5F | CTCAGTAACGTCTCT**CTC**CTTTTGATTGGCCTG |
| | m7R 5R | CAGGCCAATCAAAAG**GAG**AGAGACGTTACTGAG |
| SSM/G193L | m7R 6F | CTCTGGCCTTTTGATT**CTC**CTGTCCTATGGCCT |
| | m7R 6R | AGGCCATAGGACAG**GAG**AATCAAAAGGCCAGAG |
| SSM/G197L | m7R 7F | GATTGGCCTGTCCTAT**CTC**CTCACCTACTGCTAC |
| | m7R 7R | GTAGCAGTAGGTGAG**GAG**ATAGGACAGGCCAATC |
| TSM | m7R 8F | CTCT**CTC**CTTTTGATT**CTC**CTGTCCTAT**CTC**CT |
| | m7R 8R | AG**GAG**ATAGGACAG**GAG**AATCAAAAG**GAG**AGAG |
| GZMD | m7R 9F | AACGTCTCTCTCACCTACTGCTACTCCCTCGACCTC |
| | m7R 9R | GTAGGTGAGAGAGACGTTACTGAGGAAGGAGGTCTG |

*Immunostaining of Cultured Cells*—Transfected HEK293 cells on coverslips were permeabilized with 100% methanol for 6 min at −20 °C, rinsed three times in PBS, blocked with 3% BSA in PBS containing 0.1% Triton X-100 (PBST) for 45 min, and incubated for 2 h with 7Rc rabbit polyclonal antibody (1:200 dilution) and subsequently for 1 h with fluorescein- or rhodamine-conjugated goat anti-rabbit antibody (1:200; Santa Cruz Biotechnology, Santa Cruz, CA). Next, the transfected cells were incubated for 1 h with a mouse monoclonal anti-Xpress-FITC antibody (1:100 dilution; Invitrogen). The cells were then washed three times in PBST, stained with propidium iodide or 4′,6-diamidino-2-phenylindole (DAPI) for detection of nuclei, and viewed with fluorescence microscopy.

Immunostaining for Golgi markers GM130 and TGN38 was carried out following the same protocol described above using antibodies from Abcam (Cambridge, MA) at 1:200 and 1:500 dilutions, respectively. The co-localization of these Golgi markers and wild-type and mutant RHBDD2 was quantified using the program Olympus Fluoview Version 3.0. Transfected cells were outlined to quantify the degree of overlap. Co-localization was reported as a Pearson's coefficient, which measures how well the pixels from two different color channels fit to a linear relation. The Pearson's coefficient can have values from −1 to 1 with 1 indicating absolute overlap, 0 showing that there is no co-localization, and −1 representing an inverse correlation (relatively high scores on one variable paired with relatively low scores on the other variable).

*Immunostaining of Mouse Retinal Sections*—All tissue processing, image acquisition, and analysis procedures were as described (23–25). Central sections (10 $\mu$m thick; three nonadjacent sections per slide) were located 200–400 $\mu$m from the optic nerve. Before immunofluorescence staining, the sections were incubated with the same primary and secondary antibodies described in the previous section. To show the co-localization of RHBDD2 with both cone and Müller cells, sections were also incubated with cone opsin antibodies (short wavelength-sensitive opsin (S opsin) (OS2) and midwavelength-sensitive opsin (M opsin) (COS1) kindly provided by Dr. Agoston Szél, Semmelweis University Medical School, Budapest, Hungary) and glutamine synthetase antibody (1:5000; Sigma-Aldrich G2781, rabbit polyclonal), respectively, with the corresponding secondary antibodies. Confocal images were acquired using a Leica TCS SP2 laser-scanning confocal microscope (Leica Microsystems, Exton, PA). Images were processed using Adobe Photoshop software. The results shown are representative of five separate immunolabeling experiments from three different adult C57BL/6 mouse retinas.

For unknown reasons, retinal sections incubated with GM130 antibody in the conditions used for cultured HEK293 cells showed no results. Therefore, we obtained retinal sections following the fixation times and temperatures described by Kerov *et al.* (26). Briefly, the enucleated mouse eyes were poked through the cornea with a 21-gauge needle and fixed with 4% paraformaldehyde in PBS for 1 h at 25 °C. After fixation and removal of the cornea and lens, the eyes were hemisected, submersed in a 30% sucrose solution in PBS for 5 h at 48 °C, then embedded in OCT, frozen, and sectioned. The 10-$\mu$m sections were incubated for 2 h with 7Rc (1:200 dilution) and GM130 antibody (1:50 dilution) and subsequently for 1 h with Alexa Fluor 488 goat anti-rabbit or Alexa Fluor 568 goat anti-mouse secondary antibodies (1:500; Invitrogen).

*Screening the DNA of Patients with Retinal Degenerations for Variants in the RHBDD2 Gene*—The DNA of 110 unrelated patients of mixed ethnicities who were diagnosed with various retinal diseases such as cone dystrophy, cone-rod dystrophy, Stargardt disease, and autosomal dominant and recessive retinitis pigmentosa was screened for variants in the *RHBDD2* gene. The DNA of 95 control individuals with similar ethnic distribution (56% white, 15% black, 22% Asian, and 7% Hispanic) was also screened for *RHBDD2* variants. PCR products resulting from the targeted amplification of *RHBDD2* coding sequences were subjected to dideoxy sequencing and analyzed using Sequencher software (Gene Codes Corp., Ann Arbor, MI).

## RESULTS

*Cloning and Characterization of the Rhbdd2 cDNA*—To identify novel cone photoreceptor genes, we carried out representational difference analysis using mRNAs from adult cone degeneration (*cd*) and normal dog retinas as described previously (27). One of the clones isolated in the screen was predicted to encode a part of a protein containing the rhomboid domain. With this clone as a probe, we then screened a dog retinal cDNA library and isolated an ~2.0-kb cDNA clone that appeared to have the entire open reading frame of the predicted rhomboid domain-containing protein. Using public database information, the sequence of this clone was found to be highly homologous to sequences of mRNAs from three different species: mouse (GenBank™ accession number BC018360, identified as rhomboid domain-containing 2 (*Rhbdd2*)), rat (GenBank accession number XM_341058, called rhomboid veinlet-like 7 (*Rhbdl7*)), and human (GenBank accession numbers AF226732 and BC069017, identified as *NPD007* and *RHBDD2*, respectively). We then isolated the corresponding mouse cDNA from a mouse retinal cDNA library. Because the database mouse mRNA sequence and that of our isolated mouse clone did not have an in-frame termination codon upstream of the first methionine and the N termini of the human AF226732 and rat clones encode predicted proteins that are 45 and 27 amino acids longer than BC018360, respectively, we needed to confirm whether our mouse clone was full length or a fragment. We searched for cDNAs with a longer 5′-end using 5′ RACE (rapid amplification of cDNA ends) (Invitrogen) but were unable to isolate a longer transcript after multiple attempts. Therefore, we concluded that this mRNA contains the complete ORF that encodes a protein of 361 amino acids. We also identified another mouse *Rhbdd2* transcript with the same ORF but with a very long 3′-UTR and isolated two human transcripts that are splicing variants produced by insertion of 122- or 126-bp fragments into the first intron of *RHBDD2*. Both isoforms contain a shorter ORF than that of BC069017 and code for a human protein of 223 instead of 364 amino acids. Using an InterProScan algorithm, we found that RHBDD2, an uncharacterized 39-kDa protein that is highly conserved between species, contains five transmembrane helices; however, TMpred parameters revealed seven possible transmembrane helices.

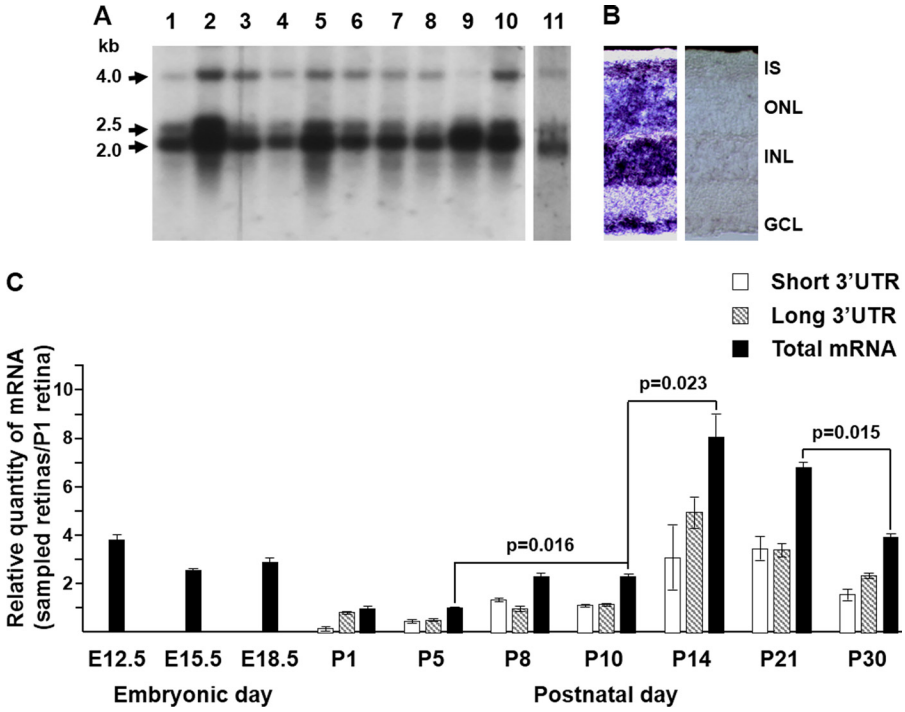


FIGURE 1. ***Rhbdd2* mRNA expression in mouse tissues and its quantification during retinal development.** *A*, a mouse multitissue Northern blot of mRNAs from heart (*lane 1*), brain (*lane 2*), liver (*lane 3*), spleen (*lane 4*), kidney (*lane 5*), embryo (*lane 6*), lung (*lane 7*), thymus (*lane 8*), testis (*lane 9*), and ovary (*lane 10*) and a separate blot containing mouse retinal mRNA (*lane 11*) were probed with a $^{32}$P-labeled *Rhbdd2* cDNA. *Arrows* indicate the sizes of the three detected transcripts (2.0, 2.5, and 4 kb), respectively. *B*, *in situ* hybridization of *Rhbdd2* mRNAs in mouse retina with antisense (*left panel*) and sense (*right panel*) DIG-labeled riboprobes. The *Rhbdd2* mRNA localized to all the nuclear layers; no signal was detected with the sense probe. *C*, quantitative RT-PCR amplification of mRNAs from mouse embryonic eyes and postnatal retinas at different times of development. Relative expression of *Rhbdd2* is normalized to the β-actin mRNA level. *Error bars* indicate S.E. *IS*, inner segment; *ONL*, outer nuclear layer; *INL*, inner nuclear layer; *GCL*, ganglion cell layer.

*Distribution of Rhbdd2 mRNA in Mouse Tissues and within the Retina*—Northern blots from different mouse tissues hybridized with the mouse *Rhbdd2* cDNA show a major transcript of ~2.0 kb in all tissues studied with very intense signals in brain, kidney, testis, and ovary and weaker bands in heart, liver, spleen, embryo, and lung (Fig. 1*A*). Two other minor transcripts, one of ~2.5 kb with tissue distribution identical to that of the 2.0-kb band, and a second of ~4.0 kb found mainly in brain, liver, kidney, and ovary but hardly present in testis, are also observed. The retinal *Rhbdd2* mRNA (*lane 11*) displays the same hybridization pattern (Fig. 1*A*). The 2.0- and 4.0-kb transcripts are in agreement with the length of the isolated *Rhbdd2* cDNAs, but the 2.5-kb mRNA had not been described previously.

*In situ* hybridization using a *Rhbdd2* antisense riboprobe to assess the expression of R*hbdd2* mRNA in mouse retina shows its presence in cell bodies located in all layers of the retina (Fig. 1*B*) as well as in the inner segments of photoreceptor cells.

To define the developmental expression pattern of *Rhbdd2* mRNA in the mouse retina, we performed qRT-PCR on mRNA from eyes of E12.5, E15.5, and E18.5 embryos and in retinas from mice at birth (P1), P5, P8, P10, P14, P21, and P30 and compared the levels at all ages with that observed at P1 (Fig. 1*C*, *black bars*). The obtained data were subjected to repeated one-way analysis of variance to check for a significant effect of time on mRNA expression. Success in the Omnibus test indeed suggested significance in the effect of time on mRNA transcription (F statistic = 7.44). Our results indicate that the amount of transcript at E12.5 is higher than at the more advanced embryonic stages, and it is very similar to that of total mRNA measured in the adult retina at P30 (Fig. 1*C*). *Rhbdd2* mRNA levels after birth (P1) and until P5 are further reduced from those at E15.5 and E18.5 and are not significantly different ($p = 0.93$). At P8 and P10, *Rhbdd2* mRNA levels are double that at P5 ($p = 0.016$). The strongest expression is observed at P14 ($p = 0.023$), and it decreases thereafter with a significant change between P21 and P30 ($p = 0.015$). We also measured by qRT-PCR the levels of the long 3′-UTR transcript at all the different postnatal developmental stages (*striped bars*) and determined the levels of the short 3′-UTR mRNAs (*white bars*) by subtraction from the total mRNA. Except for the P1 and P30 samples, both short and long 3′-UTR transcripts seem to contribute similarly to the total amount of *Rhbdd2* mRNA.

*Expression of the RHBDD2 Protein in Mouse Retina during Development*—A rabbit antiserum against RHBDD2 (referred to as 7Rc) was generated using a synthetic C-terminal peptide of RHBDD2 (ProSci Inc.). To determine the specificity of this antiserum, we prepared an Xpress-tagged RHBDD2 expression vector in the pcDNA4/HisMax plasmid (Invitrogen), which contained the predicted open reading frame of *Rhbdd2* cDNA inserted downstream of the polyhistidine ($His_6$) tag and the Xpress epitope region (Fig. 2*A*). This vector was transfected into HEK293 cells. Immunoblotting analysis of protein extracts from these cells demonstrated that 7Rc strongly bound a ~44-kDa protein, also recognized by the Xpress antibody (Fig. 2*B*). The molecular mass of this protein, ~5 kDa heavier than that estimated from the RHBDD2 primary structure (39 kDa), may result from the additional 32-amino acid vector sequence that

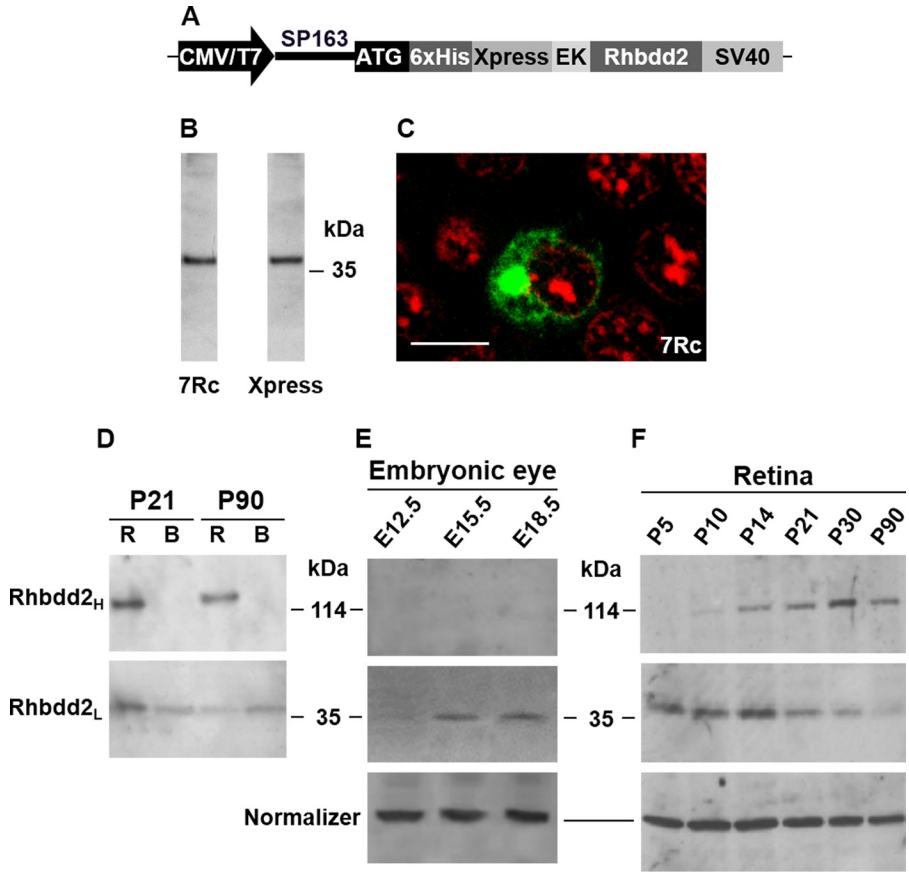


FIGURE 2. **Expression of the RHBDD2 protein in transfected HEK293 cells and in mouse embryonic eyes, postnatal retina, and brain.** *A*, schematic illustration of the pcDNA4/HisMax RHBDD2 expression construct. The vector contains the SP163 translational enhancer directly upstream of the ATG initiation codon, and the enterokinase (*EK*) cleavage site preceding the *Rhbdd2* cDNA. *B*, Western blot of a crude protein extract obtained from cultured *Rhbdd2*-transfected cells using 7Rc (*left lane*) and the Xpress antibody (*right lane*). *C*, immunocytochemical detection of the RHBDD2 protein (*green*) after transient transfection of the expression vector into HEK293 cells. Propidium iodide was used to visualize the nucleus of the cells (*red*). *Scale bar*, 15 $\mu$m. *D*, retinal and brain protein extracts (60 $\mu$g each) from P21 and P90 mice were subjected to 8% SDS-PAGE under reducing conditions followed by immunoblotting using 7Rc. The *lower panel* shows 39-kDa protein bands in both tissue samples. The 117-kDa band identified in retinal extract was absent in brain, indicating tissue specificity (*upper panel*). *R*, retina; *B*, brain. *E*, expression of RHBDD2 in mouse embryonic eyes during development. Protein extracts (50 $\mu$g) were loaded into each lane of a 4–12% gel that was subjected to SDS-PAGE, and results were normalized to $\alpha$-tubulin. *F*, Western blot of retinal extracts at different developmental times. The *upper* and *middle* blots correspond to the trimeric and monomeric forms of RHBDD2, respectively. Protein levels were normalized to $\beta$-actin.

was fused to the N-terminal region of RHBDD2 as well as from possible modification(s) of the protein. In addition, the immunocytochemical localization of RHBDD2 in transfected HEK cells using 7Rc or the Xpress antibody was identical (thus, only 7Rc staining is shown in Fig. 2*C*). The staining was strong in a distinct perinuclear region, and it resembled a bead necklace around the nucleus. Further confirmation of the specificity of 7Rc for RHBDD2 was obtained by the disappearance of all labeling in RHBDD2-transfected HEK cells incubated with 7Rc that had been preabsorbed with the polypeptide used to generate it.

Because the same *Rhbdd2* transcripts were observed in all mouse tissues studied, we initially examined the expression of the RHBDD2 protein only in retina and brain. As shown in Fig. 2*D*, 7Rc recognized the 39-kDa protein band ($RHBDD2_L$; monomer) in both tissues at P21 and P90 and an additional protein band of 117 kDa ($RHBDD2_H$; trimer) only in retinal extracts. We then tested other mouse tissues for $RHBDD2_H$ but did not detect it (data not shown).

To determine the expression of RHBDD2 from mouse retina during development, we obtained retinal protein extracts from E12.5, E15.5, and E18.5 embryonic eyes and from retinas of P5, P10, P14, P21, P30, and P90 animals and subjected them to Western blot analyses using 7Rc. Interestingly, the $RHBDD2_L$ and $RHBDD2_H$ proteins recognized by the 7Rc antibody respond in an opposing manner as mice age. The data indicate that although $RHBDD2_H$ is not seen at embryonic stages (Fig. 2*E*), only increases from P5 to P30, and remains at similar levels at P90 (Fig. 2*F*), the levels of $RHBDD2_L$ increase from E12.5 to E15.5 (Fig. 2*E*) and are thereafter similar until P14, decrease between this time and P30, and remain the same until P90 (Fig. 2*F*). Furthermore, the total level of the two retinal RHBDD2 proteins ($RHBDD2_L$ plus $RHBDD2_H$) is higher at P14 compared with other ages. This is in agreement with the expression profile of mRNA in developing retina (Fig. 1*C*).

*Golgi Localization of RHBDD2*—As seen in Fig. 2*C*, 7Rc strongly labeled the region where the Golgi apparatus resides in *Rhbdd2*-transfected HEK293 cells. Therefore, we used Golgi markers to analyze the localization of RHBDD2 in this structure of the cells. Fig. 3*A* shows that the RHBDD2 signal exhibits a high degree of overlap with the signal of the *cis*-Golgi matrix protein GM130 (Pearson's coefficient, 0.95 $\pm$ 0.01; *top panel*).

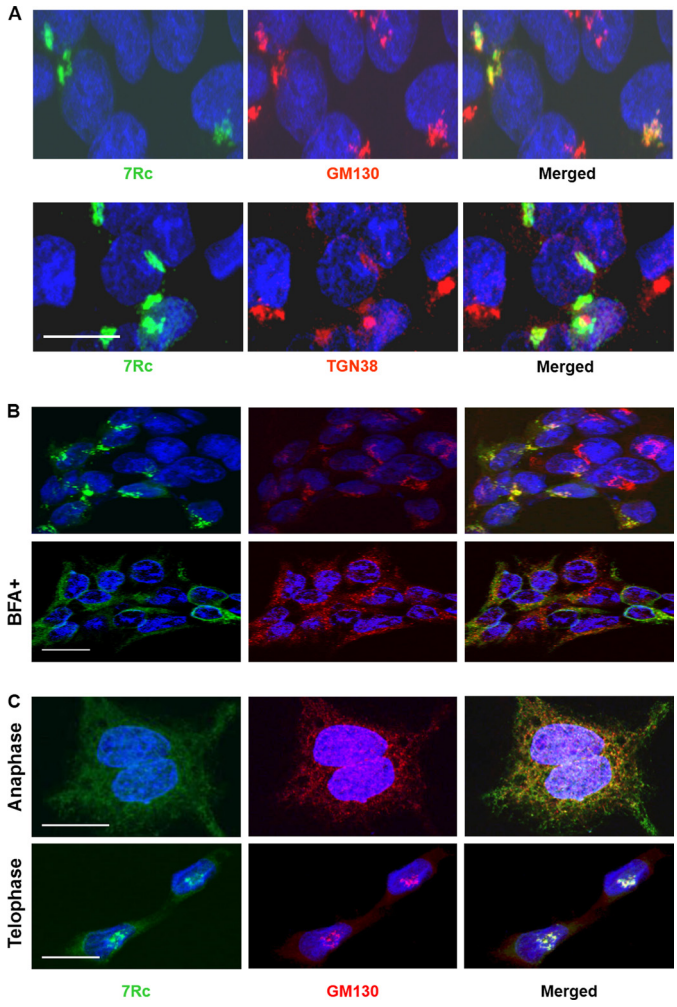


FIGURE 3. **Golgi localization of RHBDD2 in transfected HEK293 cells.** *A*, immunocytochemical detection of RHBDD2 and GM130 (*top panel*) or RHBDD2 and TGN38 (*bottom panel*) proteins after transient transfection of the *Rhbdd2* expression vector into HEK293 cells. The obtained images for each staining were merged. *Scale bar*, 15 $\mu$m. *B*, *Rhbdd2*-transfected cells with or without 50 $\mu$M BFA were incubated for 30 min at 37 °C before fixation. Cells were stained with 7Rc or anti-GM130 antibody. RHBDD2 co-localization with GM130 is sensitive to the exposure of cells to BFA. *C*, RHBDD2 and GM130 co-localize during mitosis. RHBDD2-expressing cells were fixed, permeabilized, and double stained with the same antibodies during anaphase and telophase. *Scale bars* for *B* and *C*, 10 $\mu$m.

| | |
|---|---|
| SFLSNVCGLSIGLAYGLTYCY | human |
| SFLSNVSGLLIGLSYGLTYCY | mouse |
| SFLSNVCGLSIGLAYGLTYCY | chimpanzee |
| SFLSNVCGLSIGLAYGLTYCY | orangutan |
| SFLSNVSGLLIGLSYGLTYCY | rat |
| SFLSNLCGLLIGLLYGLTNCY | guinea pig |
| SFLSNVCGLGIGLAYGLTYCY | wild boar |
| SFLSNVCGLGIGLTYGLTYCY | horse |
| SFLSNVCGLVIGLTYGVTYCY | african bush elephant |
| SFLSNVSGLVIGLTYGFTYCY | rock hyrax |
| SFLSNVCGLGIGLAYGVTYCY | flying fox |
| SFLSNVCGLCIGLSYGLTYCY | american pika |
| SFLSNVCGLGIGLTYGFTYCY | bottlenose dolphin |
| SFLSNICGLFIGFIYGLGYCS | wallaby |
| SFLSNVCGLSIGLAYKSLALS | rhesus monkey |
| SFLSNVCGLSIGLAWPHILLF | lemur |
| SFLSNVCGLGIGLAWPHLLLF | dog |
| SFLSNVCGLGVGLAWPHILLF | brown bats |
| SFLSNVCGLAIGLARPHVLLL | rabbit |
| SFLSNVCGLGVGLARHLLLLL | hedgehog |
| SLLSNLCGLLIGKAYGLGYCF | chicken |
| PVLSNVCGILVGIAYGMSGFF | xenopus tropicalis |

FIGURE 4. **The glycine zipper motif sequences in the RHBDD2 protein from different species.** The glycine zipper packing residues are highlighted in *red*, indicating the positions of the mutated Ser-185, Gly-189, Gly-193, and Gly-197, respectively.

On the other hand, 7Rc staining appears to overlap to a much lesser extent with that of anti-TGN38, a *trans*-Golgi marker protein (Pearson's coefficient, 0.32 ± 0.03; *bottom panel*). These results suggest that the overexpressed RHBDD2 is localized predominantly to the *cis*-side of the Golgi apparatus and may function in the early stages of the endosomal sorting pathway rather than during the later stages.

It has been observed before that upon treatment of cells with brefeldin A (BFA), a Golgi-destabilizing agent, the components of the *cis*-Golgi matrix intersperse in the cytoplasm and appear as puncta (28). Furthermore, other studies have demonstrated that Golgi-specific spectrins associate with Golgi membranes in a BFA-sensitive manner (29). Therefore, as an alternative approach to evaluate the Golgi localization of RHBDD2, we tested its sensitivity to BFA to examine whether BFA treatment would disrupt the association of RHBDD2 with the Golgi complex as in the case of spectrins. Fig. 3*B* shows that treatment of *Rhbdd2*-transfected HEK293 cells with BFA for 30 min results in disruption of the stacked Golgi structure, inducing a rapid spreading of RHBDD2, as demonstrated by staining with anti-GM130. This result indicates that RHBDD2 associates with the Golgi membranes and that this association is BFA-sensitive.

The structural integrity of the Golgi apparatus is compromised during mitosis as part of the normal inheritance process. We analyzed the localization of RHBDD2 in the cells during mitosis to determine in which compartment it resides. Exponentially growing and stably transfected HEK293 cells were fixed and double stained with 7Rc and anti-GM130 antibodies. Fig. 3*C* shows co-localization of RHBDD2 and GM130 even when the Golgi apparatus is dispersed during anaphase (Pearson's coefficient, 0.741 ± 0.008). In telophase, the Golgi apparatus reformed in each of the daughter cells that display a high degree of RHBDD2 and GM130 co-localization (Pearson's coefficient, 0.852 ± 0.008). These results suggest that RHBDD2 associates with Golgi membranes during the cell cycle.

As mentioned above, prediction algorithms revealed that RHBDD2 possesses potential transmembrane domains, one of which, either the fifth or the sixth (depending on the algorithm used), contains a conserved glycine zipper motif. A rigorous analysis of sequence patterns has indicated that the G*XXX*G (GG4 motif) is the most highly biased sequence motif in naturally occurring transmembrane domains. Its glycine residues are usually separated by three large (Val, Leu, and Ile) or small (Gly, Ala, and Ser) residues in the transmembrane domains (30). Among glycine zipper motifs, the (G/A/S)*XXX*G*XXX*G and G*XXX*G*XXX*(G/S/T) are the most significant (31). Analysis of RHBDD2 sequences from different species revealed that they have glycine zipper motifs that are highly conserved (Fig. 4). Furthermore, it is interesting to note that the identified sequences contain the most common glycine zippers, which

have two or more glycines and in which glycine occupies the central position (31), but that a separate set that includes those RHBDD2 sequences from human, chimpanzee, orangutan, mouse, rat, and other mammals exhibits extended glycine zipper motifs (Fig. 4, *top panel*); chicken and *Xenopus tropicalis* also contain these extended motifs. Of interest, some membrane proteins with homooligomeric bundle structures have extended glycine zipper motifs containing four glycine residues (*GXXXGXXXGXXX*G). It has been reported that mutation of one or more of these conserved glycine residues is in many cases deleterious to function (31).

To further analyze whether the glycine zipper motif in RHBDD2 is important for the packing of the protein into membranes, we used the pEGFP-N3 vector (BD Biosciences Clontech) to generate several mutant RHBDD2 proteins fused to the N terminus of EGFP and allow their localization *in vivo*. The mutant proteins had Ser-185, Gly-189, Gly-193, and Gly-197 individually or collectively (Gly-189, Gly-193, and Gly-197) substituted with leucine, disrupting the glycine zipper packing interface. We also generated a fusion protein that had amino acid residues 189–197 deleted from the RHBDD2 protein. HEK293 cells were then transfected with pEGFP-N3 containing the *Rhbdd2* or mutant cDNAs, and the expressed proteins were analyzed either by the green signal from EGFP or by immunocytochemistry using 7Rc and GM130 antibodies. Our results revealed that EGFP fused to RHBDD2 did not affect localization of the RHBDD2 protein (Fig. 5*A*) and that each of the Ser/Gly-to-Leu SSMs behaved differently (Fig. 5*B*). Changes in protein distribution as well as the lack of co-localization with GM130 were most notable for the G189L (Pearson's coefficient, 0.22 ± 0.01) and the G193L mutants (Pearson's coefficient, 0.31 ± 0.02). In contrast, the S185L and G197L mutants did not induce significant changes (Pearson's coefficients, 0.70 ± 0.04 and 0.69 ± 0.02, respectively). Surprisingly, RHBDD2 carrying the three Gly-to-Leu substitutions had a stronger co-localization with GM130 (Pearson's coefficient, 0.42 ± 0.01; Fig. 5*C*, *TSM*) than the G189L and G193L SSMs. The mutant resulting from the deletion of the amino acid residues 189–197 did not co-localize with GM130 (Pearson's coefficient, 0.14 ± 0.07; Fig. 5*C*, *GZMD*), but because we noticed that the green fluorescence excitation of this motif-deleted protein faded very fast, we used 7Rc to detect its localization (Fig. 5*C*, *GZMD*). In both cases, a dispersion of RHBDD2 in the cytoplasm was observed, indicating a dislodgment of RHBDD2 from the Golgi apparatus and suggesting that RHBDD2 might be anchored on this organelle. To support this idea, we next fractionated by ultracentrifugation the subcellular organelles/membrane vesicles of retinal tissue using a discontinuous sucrose gradient as described by Gangalum *et al.* (32). Western blots of the fractions were then incubated with 7Rc and GM130 antibodies. The results indicate that only the $S_2$ fraction (the Golgi membrane fraction) contains an appreciable amount of RHBDD2 protein and that upon recentrifugation of $S_2$ a significant amount of RHBDD2 can be found in the stacked Golgi fraction 3 (Fig. 6*A*, $SGF_3$), further supporting that RHBDD2 is localized to the Golgi apparatus of retinal cells.

Immunohistochemistry experiments confirmed that RHBDD2 and GM130 co-localize in the retina. Double stained images

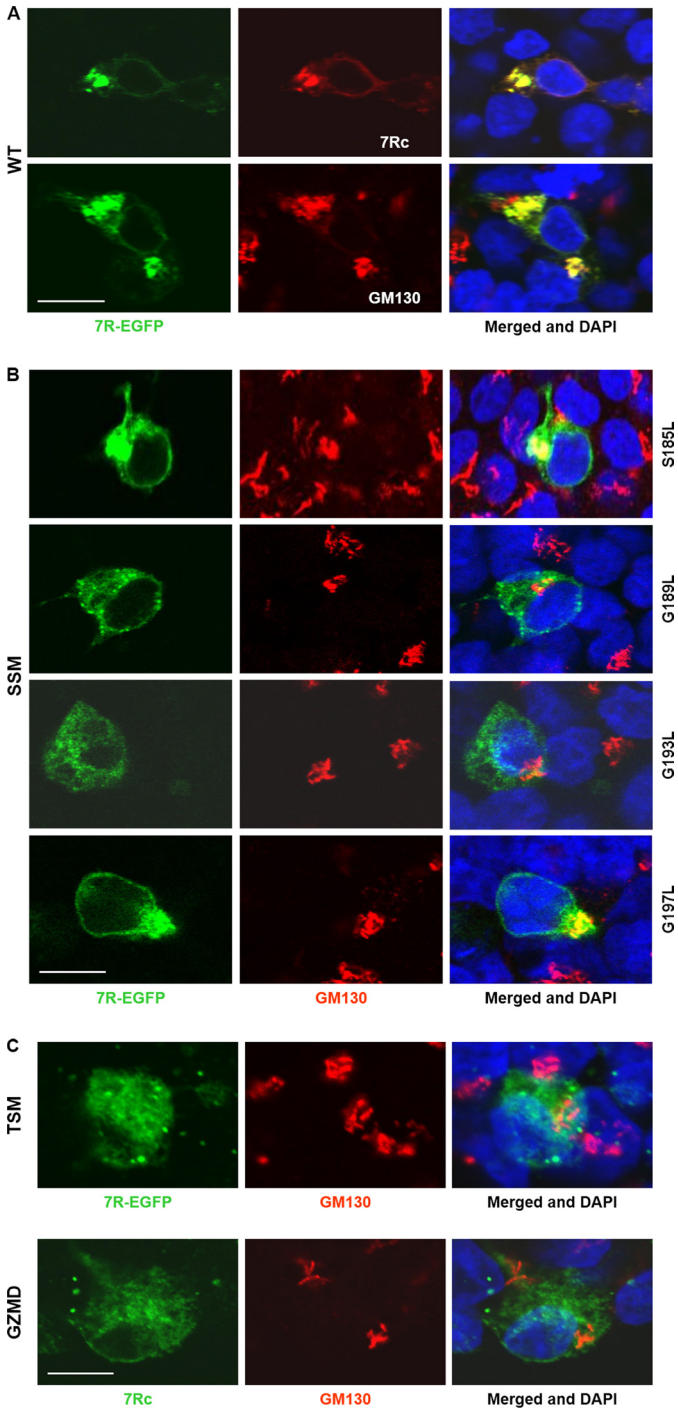


FIGURE 5. **Subcellular localization of RHBDD2 glycine zipper mutants.** HEK293 cells were transfected with *Rhbdd2*-EGFP or *Rhbdd2*-EGFP mutants and stained with 7Rc or double stained with 7Rc and GM130. The cells were transfected with vector containing a wild-type (WT) *Rhbdd2* cDNA together with green fluorescent protein used as a control for experiments and to monitor transfection efficiency (*A*); S185L, G189L, G193L, and G197L SSMs (*B*); a G189L, G193L, and G197L triple substitution mutant (*TSM*) (*C*); and the glycine zipper motif (amino acids 189–197) deletion mutant (*GZMD*) (*D*). Immunofluorescence imaging was performed to verify the expression and distribution of RHBDD2-EGFP mutants. *Scale bars*, 15 $\mu$m.

obtained using antibodies against RHBDD2 and GM130 (Fig. 6*B*) show the co-localization of these proteins in the inner segment of photoreceptor cells (Pearson's coefficient, 0.48 ± 0.03), mainly in cone inner segments, as well as in the perinuclear

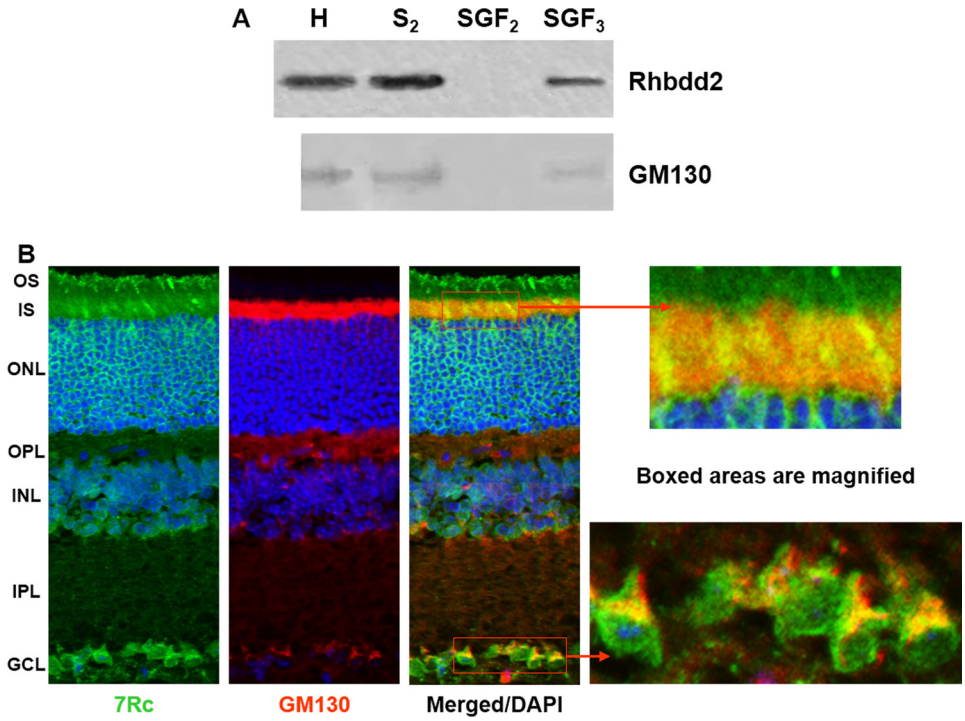


FIGURE 6. **Fractionation of mouse retinal protein extract and co-localization of RHBDD2 with a Golgi marker.** *A*, the postnuclear supernatants were fractionated on discontinuous sucrose gradients. Western blots incubated with 7Rc and GM130 antibody show that the $S_2$ fraction contains a substantial amount of RHBDD2 protein; upon recentrifugation of $S_2$, a significant amount of RHBDD2 is found in the stacked Golgi fraction 3 ($SGF_3$). *H*, homogenate. *B*, confocal microscopic images of adult mouse retinal sections stained with 7Rc, GM130 antibody, and DAPI. The merged image illustrates co-localization of these two proteins. The *far right panel* shows the magnified *boxed* areas. *OS*, outer segment; *IS*, inner segment; *ONL*, outer nuclear layer; *OPL*, outer plexiform layer; *INL*, inner nuclear layer; *IPL*, inner plexiform layer; *GCL*, ganglion cell layer.

region of ganglion cells (a stronger Pearson's coefficient, 0.67 ± 0.05, similar to what was seen in transfected HEK293 cells. In addition, very weak signals were observed on the inner nuclear layer edges bordering the outer plexiform layer and inner plexiform layer.

*Specific Pattern of RHBDD2 Immunoreactivity in Developing and Adult Mouse Retina*—We used immunohistochemistry to follow the expression of RHBDD2 in mouse retina during development from E12.5 to adulthood (Figs. 7 and 8). Our results show that the distribution of RHBDD2 is more complex than our previous *in situ* hybridization data suggested (Fig. 1*B*). We detected a weak but clearly positive signal in E10.5 (data not shown), the youngest tissue in which we examined RHBDD2 expression, although it is possible that the RHBDD2-positive cells appear at an even younger age. A stronger signal is observed at E12.5, and the intensity of the staining increases in E15.5 and E18.5 retinas. At these embryonic stages, all cells are positive for RHBDD2 (Fig. 7*A*). The gradual, age-dependent appearance of the RHBDD2 protein in the layers of the retina begins at birth and continues throughout development (Fig. 7*B*). At postnatal day 1, a small number of positive cells are observed at the level of the ganglion cell layer (GCL) and in the inner edge of the ventricular zone of the retina. Between P1 and P5, the labeling of RHBDD2 shows a similar spatial pattern, but by P8 to P11, immunostaining has progressively increased and entirely occupies the GCL and inner nuclear layer. However, no significant RHBDD2 immunoreactivity is observed in the photoreceptor cell bodies of the outer nuclear layer (ONL). At P21, RHBDD2 is localized to all nuclear layers of the retina (Fig. 7*B*).

In the ONL, the RHBDD2 signal is primarily present in the cytoplasm of the cell soma adjacent to the plasma membrane of the photoreceptor cells, and it is different from that observed in embryonic and early retinal developmental stage cells where it is localized both in the nucleus and cytoplasm. The consistent perinuclear signal present in the later ages may suggest that compartmentalization is an essential process for the normal functioning of RHBDD2 in more mature retina. Interestingly, a small number of strongly stained RHBDD2 cells with very short outer segments (OS) and an irregular distribution first appear in the outer retina at P12 (Fig. 8*A*). To determine the identity of these RHBDD2-positive cells, we double labeled the photoreceptors of the mouse retina at P13–14 with both 7Rc and antibodies against S opsin, which is abundant in the cones of the mouse ventral retina, or M opsin, which is concentrated in the dorsal retina cones (33). Our results showed that RHBDD2 immunoreactivity consistently co-localized with S and M opsins in the OS of both types of cones (Fig. 8*B*, only M opsin is shown).

The characteristics of RHBDD2 staining in the ONL were seen more thoroughly with confocal microscopy images of adult retinal sections. Fig. 8*C* shows that all photoreceptor cells stained positive for RHBDD2; however, a small number of short OS were stained with 7Rc. These OS corresponded to cells that after differentiation and migration aligned near the outermost region of the ONL; their nuclei contained several clumps of irregularly shaped heterochromatin. The positional and morphological characteristics of these cells are hallmarks of mature cone photoreceptors (34, 35). As also seen in Fig. 8*C*, RHBDD2

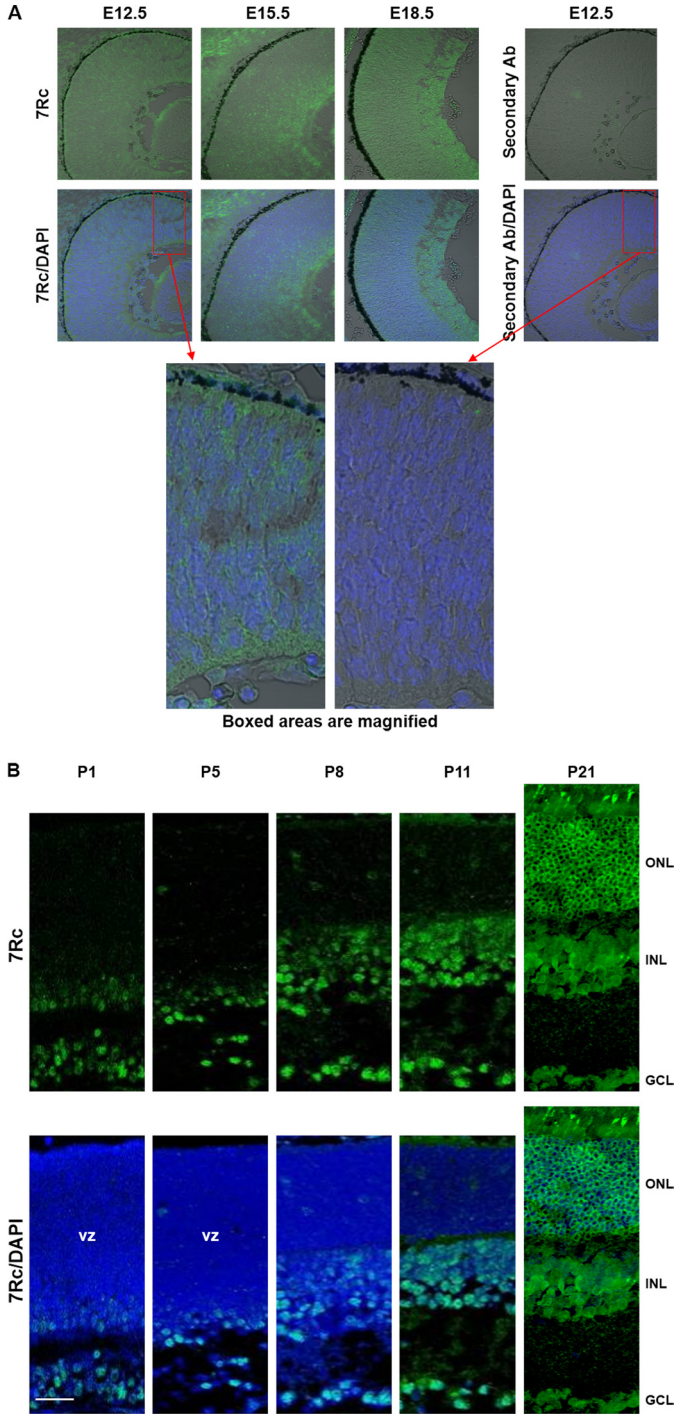


FIGURE 7. **RHBDD2 immunoreactivity during development of mouse retina.** *A*, at E12.5, E15.5, and E18.5, RHBDD2 is ubiquitously expressed in all retinoblasts, and the intensity of the signal increases with age. The *right panel* is a section from an E12.5 eye stained only with the secondary antibody (*Ab*), demonstrating the specificity of the primary antibody signal. The *bottom panels* show the magnified *boxed* areas. *B*, at P1 and P5, RHBDD2 is expressed in some cells of the ventricular zone (*vz*) and in the GCL. At P8 and P11, immunostaining is clearly detected in the GCL, inner nuclear layer (*INL*), and in some cells of the ONL. By P21, RHBDD2 is localized to all retinal nuclear layers. In the ONL, RHBDD2 is mainly present around the nuclei of photoreceptors. *Scale bar*, 20 $\mu$m.

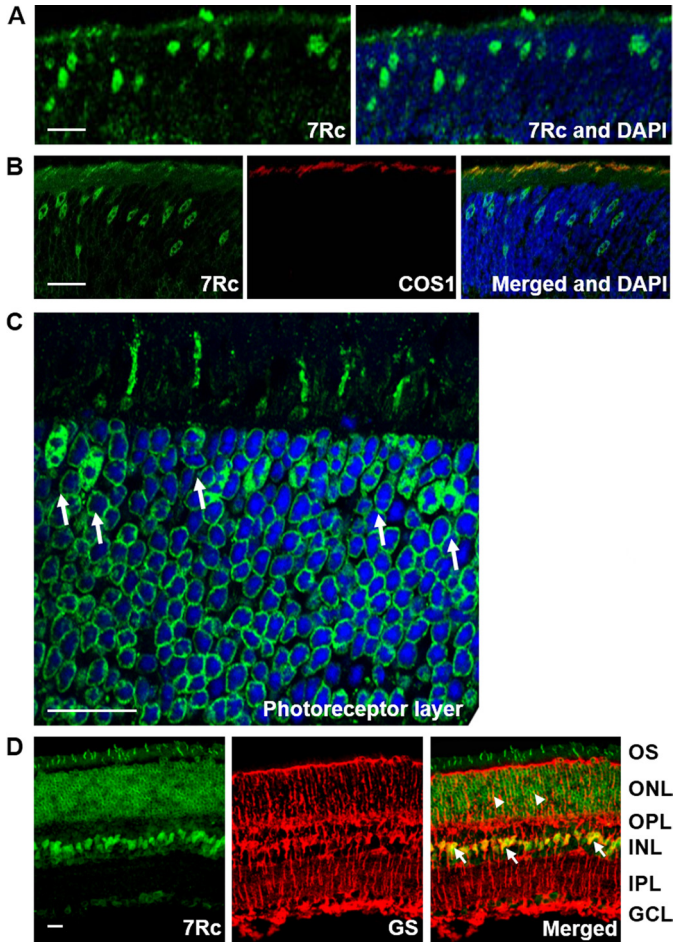


FIGURE 8. **Detection of RHBDD2 expression in young and adult mouse retina sections.** *A*, section of a 12-day-old mouse retina stained with 7Rc-FITC and DAPI, which was used to stain the nuclei. The photoreceptor layer shows strongly stained cone cell nuclei migrating toward the outer edge of ONL and short outer segments. *B*, a 12-day-old mouse retinal section triple stained with 7Rc tagged with FITC, the cone marker COS1 tagged with Alexa Fluor 647, and DAPI. The merged image shows overlapping RHBDD2 and COS1 staining. *C*, a magnified image of the ONL from an adult retinal section immunolabeled with 7Rc. The *arrows* point to the larger, oval nuclei of cones that appear to contain several clumps of irregularly shaped heterochromatin. *D*, images of an adult retina showing RHBDD2 localization (*green*), glutamine synthetase (*GS*) localization (*red*), and their co-localization in the somas of many Müller glial cells (*arrows*) and some of their processes (*arrowheads*). *Scale bars*, 20 $\mu$m. *INL*, inner nuclear layer; *OPL*, outer plexiform layer; *IPL*, inner plexiform layer.

immunostaining was restricted to the cytoplasm surrounding the nuclei, but we were unable to determine whether it was or was not on the nuclear membranes.

In addition to the photoreceptors, the staining pattern of RHBDD2 in adult retinas showed strong RHBDD2 expression in the GCL and inner nuclear layer. In the latter, a small number of cells were more intensively labeled than others. Double labeling with 7Rc and the Müller cell marker glutamine synthetase antibody revealed co-localization of RHBDD2 and glutamine synthetase in these same cells, identifying them as Müller cells (Fig. 8*D*, *arrows*). Very weak co-localization also was present on some radial processes of Müller cells in the ONL (*arrowheads*).

*A Missense Mutation in RHBDD2 Co-segregates with Disease in a Family Affected with arRP*—A systematic mutational analysis was initiated to determine whether there are disease-causing mutations in the human *RHBDD2* gene. We screened the DNA of a small group of patients with different types of retinal degeneration by direct DNA sequence analysis of all exons and exon-intron boundaries and found variants of *RHBDD2* in arRP

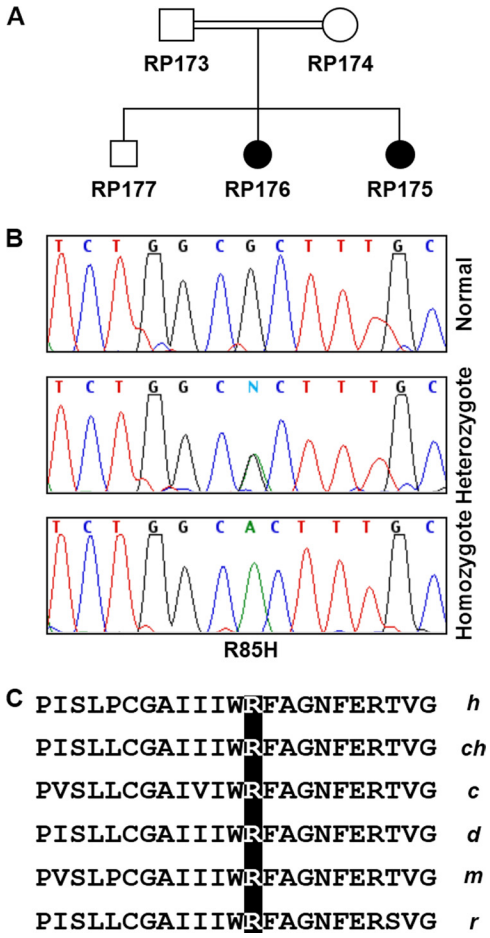


FIGURE 9. **R85H mutation in the human *RHBDD2* gene.** *A*, pedigree of an arRP family carrying the R85H mutation in the *RHBDD2* gene. *Filled circles* represent the affected members of the family. *B*, sequences of DNA fragments containing the site of mutation in the *RHBDD2* gene. *C*, Arg-85 is conserved in the RHBDD2 sequence among different species of mammals. *h*, human; *ch*, chimpanzee; *c*, cow; *d*, dog; *m*, mouse; *r*, *rat*.

patients. One of them, proband RP176 (Fig. 9*A*), had a G to A transition in exon 2 that changed arginine to histidine at codon 85 (Fig. 9*B*). This R85H allele co-segregated with the clinical phenotype in the patient's family. In addition, 95 control individuals (190 chromosomes) did not carry the R85H mutation. Arg-85 is located in the intracellular loop between the second and third predicted transmembrane domains of the RHBDD2 protein and is highly conserved among human, chimpanzee, cow, dog, mouse, rat, and many more species (Fig. 9*C*). Interestingly, in another unrelated individual, two different *RHBDD2* transcripts were identified: a wild-type mRNA and a second transcript containing a 7-nucleotide deletion in exon 2 of *RHBDD2* that leads to a frameshift and the creation of a premature stop codon. This individual also had a common single nucleotide polymorphism (SNP) at the −13 position upstream of exon 2. Unfortunately, no other family members are available for testing to determine whether the deletion is linked to any disease phenotype. We excluded the known disease-causing genes *PDE6A*, *PDE6B*, *RPE65*, *ABCA4*, and *TULP1* from all the families studied using linkage analysis. All patients' DNAs were also screened for the *CRX*, *RDS*, *NR2E3*, and *RHO* genes, and no mutations were found.

## DISCUSSION

Herein, we identified a cDNA encoding RHBDD2, a novel rhomboid-like protein, in a screen for mRNAs present in cone photoreceptors. However, we found *Rhbdd2* transcripts in all major mouse tissues. The expressed RHBDD2 is an intramembrane protein with a localization restricted to the Golgi apparatus in transfected HEK293 cells. Retina is the only tissue where we have detected two forms of the RHBDD2 protein, $RHBDD2_L$ and $RHBDD2_H$, which most likely is an $RHBDD2_L$ trimer. Inspection of databases indicates that RHBDD2 is conserved among species.

This study is the first to examine the developmental profile and cellular localization of RHBDD2 in mouse retina. We found that RHBDD2 is expressed in early life (with immunoreactivity observed at E10.5) and becomes widespread and differentially distributed after all the retinal layers have formed. The lowest levels of RHBDD2 were seen at the beginning of postnatal life, and the maximum level was observed at P14.

At P1, RHBDD2 immunoreactivity is strongest in the GCL, and it spreads during development from the inner to the outer retina. In the ONL, the first cells stained by 7Rc are detected at P12 and are somewhat scattered. By P21, RHBDD2 is all over the retina, and it appears in many neuronal and glial Müller cells. Quantification of the expression of the two different forms of RHBDD2 indicated that $RHBDD2_L$ minimally changed during development until P14 and then decreased as the age of the mouse progressed, whereas $RHBDD2_H$ increased from P5 to P30 and remained close to this level thereafter.

One of the interesting issues concerning RHBDD2 expression is the appearance of homomultimers of this protein. Our results provide evidence that $RHBDD2_L$ exists as a monomer in the inner retina neurons and the soma of photoreceptors, whereas $RHBDD2_H$ seems to be found exclusively as a polymer in cone OS. Indeed, the levels of $RHBDD2_H$ increase precisely at the time in development when the outer segments are elongating. We consider that $RHBDD2_H$ is a trimer of $RHBDD2_L$ because of its molecular mass and because it is recognized by 7Rc, a specific antibody for both forms of the RHBDD2 protein. $RHBDD2_H$ detection is not appreciably altered by increasing mercaptoethanol/DTT, treating with different concentrations of SDS before electrophoresis, or boiling the samples before loading them on the gel. $RHBDD2_H$ is present in S and M cone outer segments. It is most likely that the $RHBDD2_L$ monomer is conserved between species.

Because the biochemical functions of RHBDD2 have not been determined and establishing them will require a more complete understanding of the protein, currently, we can only speculate that $RHBDD2_H$ may be involved in the growth and maturation of the cone OS, whereas $RHBDD2_L$ may be an active participant in the early development of retinal cells. The generation of RHBDD2 knock-out mice will provide evidence for the role of RHBDD2 in these processes.

As shown in Figs. 3 and 5, the recombinant RHBDD2 localized to the Golgi apparatus of HEK293 cells. Furthermore, in retinal sections, co-localization of RHBDD2 and the Golgi marker GM130 is clearly seen at the inner segment of photoreceptors and perinuclear region of ganglion cells (Fig. 6*B*), which

is an obvious indication of the existence of RHBDD2 in the Golgi apparatus. This organelle is considered to be a distribution and shipment center for proteins and lipids inside the cell as well as for their export out of the cell. In recent years, discoveries have indicated that the Golgi complex can also be considered as a center of operations where cargo sorting/processing, basic metabolism, signaling, and cell fate decisional processes converge (36). Interestingly, cells overexpressing RHBDD2 had a compacted Golgi similar to that observed in non-transfected cells with normal reticular morphology. While performing transfection experiments with constructs containing different RHBDD2 glycine zipper mutations, we noticed that for some expressed mutant proteins the staining pattern of RHBDD2 was altered, but the Golgi remained intact. Because it is known that glycine zipper motif structures are directly involved in helix interactions, the existence of the G*XXX*G sequence in RHBDD2 suggests that this motif may not only be involved in the high affinity association of transmembrane helices but also in the association of RHBDD2 with the Golgi apparatus. In addition, our results suggest that the glycine zipper motif may play an important role in the oligomerization of RHBDD2 in OS of photoreceptors. The observation that RHBDD2 localization to the Golgi complex is glycine zipper motif-dependent even though there are no links between the function of RHBDD2 and the Golgi apparatus generates the appealing hypothesis that the formation of the trimer in outer segments of adult retina also relies on the glycine zipper motif.

Our studies also have provided evidence supporting the role of the *RHBDD2* gene, which is localized on chromosome 7q11, in the pathogenesis of retinitis pigmentosa, an inherited retinal disease that results in the loss of photoreceptors and is characterized by pigment deposits predominantly in the peripheral retina. To date, 43 genes and 50 loci have been identified for autosomal dominant, autosomal recessive, and X-linked forms of non-syndromic retinitis pigmentosa (RetNet, The Retinal Information Network). We found a homozygous mutation in the *RHBDD2* gene, R85H, that co-segregates with disease in a family affected with arRP but that does not exist in 95 controls. No other gene of the several that we investigated showed any mutation in the affected members of this family. Thus, it is possible that the *RHBDD2* gene is a new disease-causing gene and that 7q11 is a new locus for arRP. Several studies suggest that arginine residues may form salt bridges with acidic residues to stabilize protein structure, bind cofactors, or interact with DNA (37–39). The observed substitution of His for Arg at position 85 may thus disrupt the structure of the RHBDD2 protein.

Recently, Abba *et al.* (40) determined that the *RHBDD2* mRNA and its expressed protein are significantly elevated in breast carcinomas as compared with normal breast tissue samples or benign breast lesions with overexpression predominantly observed in advanced stages and that silencing of *RHBDD2* expression results in a decrease of cell proliferation. The authors showed a strong association between high *RHBDD2* expression and decreased overall survival, relapse-free survival, and metastasis-free intervals in patients with primary estrogen receptor-negative breast carcinomas. They suggested that *RHBDD2* overexpression behaves as an indicator of poor prognosis and may play a role in facilitating breast cancer progression. Also, they recognized two *RHBDD2* alternatively spliced mRNA isoforms expressed in breast cancer cell lines (40). We have found that these two isoforms are also expressed in normal retinal tissue samples. In addition, we identified a third isoform of *RHBDD2* from human retinal samples, the rhomboid domain-containing 2, transcript variant 3.

Although Abba *et al.* (40) present solid mRNA data indicating strong correlation between expression of *RHBDD2* transcripts and breast carcinomas, their Western blot and immunohistochemistry results are contrary to our results on RHBDD2. First, the polyclonal antibody that these authors used was raised against peptides that were synthesized based on the RHBDD2 protein sequence (NCBI Reference Sequence NP_065735) corresponding to residues 30–43, 253–266, and 393–406. However, the record for NP_065735 has been permanently removed from the database because this sequence is a nonsense-mediated mRNA decay candidate. Second, these three peptide sequences are encoded by the ORF of human *NPD007* mRNA (GenBank accession number AF226732) but are not found in the RHBDD2 protein sequence. *NPD007* mRNA codes for a protein with an N terminus 45 amino acids longer than RHBDD2. Peptide 30–43 is located in those 45 amino acids. Also, the *NPD007* sequence is missing two nucleotides after position 724 (G and C), which leads to a reading frame change and the creation of a new protein. The 253–266 and 393–406 peptides are located in the diverging sequence downstream of the two missing nucleotides. This is why these peptides are not present in the RHBDD2 sequence. Third, from the Western blot analysis of normal and breast cancer cell lines using their polyclonal antibody, the authors identified a 47-kDa product that they assume is encoded by isoform1 as well as a smaller protein of ~40 kDa, a product of isoform2. However, the sequences presented by the authors in Fig. 3D of their study (40) contain an ORF encoding 223 amino acids for isoform1 and 364 amino acids for isoform2. Consequently, isoform1 would code for a much smaller protein than that encoded by isoform2. Therefore, it is not clear what proteins the authors are detecting with the polyclonal antibody that they generated. These proteins are definitely different from RHBDD2.

Very recently, a study has been published describing the possible role of RHBDD2 in colorectal cancer progression. The authors indicate that expression of RHBDD2 significantly increases in advanced stages of colorectal cancer. Also, they found a significant increase of RHBDD2 mRNA and protein after treatment with the chemotherapy agent 5-fluorouracil (41).

In conclusion, we have characterized RHBDD2, a ubiquitously expressed transmembrane rhomboid-like protein associated with the Golgi apparatus that exists as a monomer in all retinal cells and as a trimer only in retinal photoreceptor outer segments, mainly in cones. Our genetic findings indicate that a mutation in the *RHBDD2* gene may lead to arRP. The association of *RHBDD2* abnormalities with diseases like neurodegenerative retinitis pigmentosa and cancer is intriguing. The unknown function of the RHBDD2 protein in mammals together with the undiscovered molecular pathways in which RHBDD2 may participate in human disorders further substantiates future studies to determine the potential role of RHBDD2 in normal cells and tissues.

## REFERENCES


1. Brown, M. S., Ye, J., Rawson, R. B., and Goldstein, J. L. (2000) Regulated intramembrane proteolysis: a control mechanism conserved from bacteria to humans. *Cell* **100,** 391–398
2. Urban, S., and Freeman, M. (2003) Substrate specificity of rhomboid intramembrane proteases is governed by helix-breaking residues in the substrate transmembrane domain. *Mol. Cell* **11,** 1425–1434
3. Weihofen, A., and Martoglio, B. (2003) Intramembrane-cleaving proteases: controlled liberation of proteins and bioactive peptides. *Trends Cell Biol.* **13,** 71–78
4. Wolfe, M. S., and Kopan, R. (2004) Intramembrane proteolysis: theme and variations. *Science* **305,** 1119–1123
5. Ha, Y. (2009) Structure and mechanism of intramembrane protease. *Semin. Cell Dev. Biol.* **20,** 240–250
6. Urban, S. (2009) Making the cut: central roles of intramembrane proteolysis in pathogenic microorganisms. *Nat. Rev. Microbiol.* **7,** 411–423
7. Mayer, U., and Nüsslein-Volhard, C. (1988) A group of genes required for pattern formation in the ventral ectoderm of the *Drosophila* embryo. *Genes Dev.* **2,** 1496–1511
8. Bier, E., Jan, L. Y., and Jan, Y. N. (1990) Rhomboid, a gene required for dorsoventral axis establishment and peripheral nervous system development in *Drosophila melanogaster*. *Genes Dev.* **4,** 190–203
9. Wasserman, J. D., Urban, S., and Freeman, M. (2000) A family of rhomboid-like genes: *Drosophila* rhomboid-1 and roughoid/rhomboid-3 cooperate to activate EGF receptor signaling. *Genes Dev.* **14,** 1651–1663
10. Lee, J. R., Urban, S., Garvey, C. F., and Freeman, M. (2001) Regulated intracellular ligand transport and proteolysis control EGF signal activation in *Drosophila*. *Cell* **107,** 161–171
11. Urban, S., and Wolfe, M. S. (2005) Reconstitution of intramembrane proteolysis *in vitro* reveals that pure rhomboid is sufficient for catalysis and specificity. *Proc. Natl. Acad. Sci. U.S.A* **102,** 1883–1888
12. Maegawa, S., Ito, K., and Akiyama, Y. (2005) Proteolytic action of GlpG, a rhomboid protease in the *Escherichia coli* cytoplasmic membrane. *Biochemistry* **44,** 13543–13552
13. Lemberg, M. K., and Freeman, M. (2007) Functional and evolutionary implications of enhanced genomic analysis of rhomboid intramembrane proteases. *Genome Res.* **17,** 1634–1646
14. Freeman, M. (2009) Rhomboids: 7 years of a new protease family. *Semin. Cell Dev. Biol.* **20,** 231–239
15. Srinivasan, P., Coppens, I., and Jacobs-Lorena, M. (2009) Distinct roles of *Plasmodium* rhomboid 1 in parasite development and malaria pathogenesis. *PLoS Pathog.* **5,** e1000262
16. Morahan, B. J., Sallmann, G. B., Huestis, R., Dubljevic, V., and Waller, K. L. (2009) *Plasmodium falciparum*: genetic and immunogenic characterisation of the rhoptry neck protein PfRON4. *Exp. Parasitol.* **122,** 280–288
17. Cowman, A. F., and Crabb, B. S. (2006) Invasion of red blood cells by malaria parasites. *Cell* **124,** 755–766
18. Whitworth, A. J., Lee, J. R., Ho, V. M., Flick, R., Chowdhury, R., and McQuibban, G. A. (2008) Rhomboid-7 and HtrA2/Omi act in a common pathway with the Parkinson's disease factors Pink1 and Parkin. *Dis. Model. Mech.* **1,** 168–174
19. Walder, K., Kerr-Bayles, L., Civitarese, A., Jowett, J., Curran, J., Elliott K, Trevaskis J, Bishara, N., Zimmet, P., Mandarino, L., Ravussin, E., Blangero, J., Kissebah, A., and Collier, G. R. (2005) The mitochondrial rhomboid protease PSARL is a new candidate gene for type 2 diabetes. *Diabetologia* **48,** 459–468
20. Adrain, C., Zettl, M., Christova, Y., Taylor, N., and Freeman, M. (2012) Tumor necrosis factor signaling requires iRhom2 to promote trafficking and activation of TACE. *Science* **335,** 225–228
21. McIlwain, D. R., Lang, P. A., Maretzky, T., Hamada, K., Ohishi, K., Maney, S. K., Berger, T., Murthy, A., Duncan, G., Xu, H. C., Lang, K. S., Häussinger, D., Wakeham, A., Itie-Youten, A., Khokha, R., Ohashi, P. S., Blobel, C. P., and Mak, T. W. (2012) iRhom2 regulation of TACE controls TNF-mediated protection against Listeria and responses to LPS. *Science* **335,** 229–232
22. Lerner, L. E., Peng, G. H., Gribanova, Y. E., Chen, S., and Farber, D. B. (2005) Sp4 is expressed in retinal neurons, activates transcription of photoreceptor-specific genes, and synergizes with Crx. *J. Biol. Chem.* **280,** 20642–20650
23. Saghizadeh, M., Gribanova, Y., Akhmedov, N. B., and Farber, D. B. (2011) ZBED4, a cone and Müller cell protein in human retina, has a different cellular expression in mouse. *Mol. Vis.* **17,** 2011–2018
24. Johnson, J. E., Jr., Perkins, G. A., Giddabasappa, A., Chaney, S., Xiao, W., White, A. D., Brown, J. M., Waggoner, J., Ellisman, M. H., and Fox, D. A. (2007) Spatiotemporal regulation of ATP and $Ca^{2+}$ dynamics in vertebrate rod and cone photoreceptor ribbon synapses. *Mol. Vis.* **13,** 887–919
25. Giddabasappa, A., Hamilton, W. R., Chaney, S., Xiao, W., and Johnson, J. E. (2011) Low-level gestational lead exposure increases retinal progenitor cell proliferation and rod photoreceptor and bipolar cell neurogenesis in mice. *Environ. Health Perspect.* **119,** 71–77
26. Kerov, V. S., Natochin, M., and Artemyev, N. O. (2005) Interaction of transducin-$\alpha$ with LGN, a G-protein modulator expressed in photoreceptor cells. *Mol. Cell. Neurosci.* **28,** 485–495
27. Saghizadeh, M., Akhmedov, N. B., Yamashita, C. K., Gribanova, Y., Theendakara, V., Mendoza, E., Nelson, S. F., Ljubimov, A. V., and Farber, D. B. (2009) ZBED4, a BED-type zinc-finger protein in the cones of the human retina. *Invest. Ophthalmol. Vis. Sci.* **50,** 3580–3588
28. Chiu, C. F., Ghanekar, Y., Frost, L., Diao, A., Morrison, D., McKenzie, E., and Lowe, M. (2008) ZFPL1, a novel ring finger protein required for *cis*-Golgi integrity and efficient ER-to-Golgi transport. *EMBO J.* **27,** 934–947
29. Gough, L. L., Fan, J., Chu, S., Winnick, S., and Beck, K. A. (2003) Golgi localization of Syne-1. *Mol. Biol. Cell* **14,** 2410–2424
30. Senes, A., Gerstein, M., and Engelman, D. M. (2000) Statistical analysis of amino acid patterns in transmembrane helices: the GxxxG motif occurs frequently and in association with $\beta$-branched residues at neighboring positions. *J. Mol. Biol.* **296,** 921–936
31. Kim, S., Jeon, T. J., Oberai, A., Yang, D., Schmidt, J. J., and Bowie, J. U. (2005) Transmembrane glycine zippers: physiological and pathological roles in membrane proteins. *Proc. Natl. Acad. Sci. U.S.A.* **102,** 14278–14283
32. Gangalum, R. K., Schibler, M. J., and Bhat, S. P. (2004) Small heat shock protein $\alpha$B-crystallin is part of cell cycle-dependent Golgi reorganization. *J. Biol. Chem.* **279,** 43374–43377
33. Szél, A., Röhlich, P., Caffé, A. R., Juliusson, B., Aguirre, G., and Van Veen, T. (1992) Unique topographic separation of 2 spectral classes of cones in the mouse retina. *J. Comp. Neurol.* **325,** 327–342
34. Carter-Dawson, L. D., and LaVail, M. M. (1979) Rods and cones in the mouse retina. I. Structural analysis using light and electron microscopy. *J. Comp. Neurol.* **188,** 245–262
35. Perkins, G. A., Ellisman, M. H., and Fox, D. A. (2003) Three-dimensional analysis of mouse rod and cone mitochondrial cristae architecture: bioenergetic and functional implications. *Mol. Vis.* **9,** 60–73
36. Wilson, C., Venditti, R., Rega, L. R., Colanzi, A., D'Angelo, G., and De Matteis, M. A. (2011) The Golgi apparatus: an organelle with multiple complex functions. *Biochem. J.* **433,** 1–9
37. Sundaralingam, M., Drendel, W., and Greaser, M. (1985) Stabilization of the central helix of troponin C by intrahelical salt bridges between charged amino acid side chains. *Proc. Natl. Acad. Sci. U.S.A.* **82,** 7944–7947
38. Llewellyn, D. H., Whatley, S., and Elder, G. H. (1993) Acute intermittent porphyria caused by an arginine to histidine substitution (R26H) in the cofactor-binding cleft of porphobilinogen deaminase. *Hum. Mol. Genet.* **2,** 1315–1316
39. Frigyes, D., Alber, F., Pongor, S., and Carloni, P. (2001) Arginine-phosphate salt bridges in protein-DNA complex: a Car-Parrinello study. *J. Mol. Struct.* (*Theochem*) **574,** 39–45
40. Abba, M. C., Lacunza, E., Nunez, M. I., Colussi, A., Isla-Larrain, M., Segal-Eiras, A., Croce, M. V., and Aldaz, C. M. (2009) Rhomboid domain containing 2 (RHBDD2): a novel cancer-related gene over-expressed in breast cancer. *Biochim. Biophys. Acta* **1792,** 988–997
41. Lacunza, E., Canzoneri, R., Rabassa, M. E., Zwenger, A., Segal-Eiras, A., Croce, M. V., and Abba, M. C. (2012) RHBDD2: a 5-fluorouracil responsive gene overexpressed in the advanced stages of colorectal cancer. *Tumour Biol.* **33,** 2393–2399